Investigation of Quantum Transport in Nanoscaled GaN High Electron Mobility Transistors

O. Baumgartner, Z. Stanojević, L[a]. Filipović, A. Grill, T. Grasser, and H. Kosina
Institute for Microelectronics, TU Wien, Gußhausstraße 27–29, 1040 Wien, Austria
Email: {baumgartner|stanojevic|lidijafilipovic|grill|grasser|kosina}@iue.tuwien.ac.at

M. Karner
Global TCAD Solutions GmbH, Landhausgasse 4/1A, 1010 Wien, Austria
Email: m.karner@globaltcad.com

***Abstract*—In this paper, a comprehensive investigation of quantum transport in nanoscaled gallium nitride (GaN) high electron mobility transistors (HEMTs) is presented. A simulation model for quantum transport in nanodevices on unstructured grids in arbitrary dimension and for arbitrary crystal directions has been developed. The model has been implemented as part of the Vienna-Schrödinger-Poisson simulation and modeling framework. The transport formalism is based on the quantum transmitting boundary method. A new approach to reduce its computational effort has been realized. The model has been used to achieve a consistent treatment of quantization and transport effects in deeply scaled asymmetric GaN HEMTs. The self-consistent electron concentration, conduction band edges and ballistic current have been calculated. The effects of strain relaxation at the heterostructure interfaces on the potential and carrier concentration have been shown.**

I. Introduction

Gallium nitride based high electron mobility transistors have garnered increasing interest in recent years as viable candidates for high power and high frequency applications [1]. They offer high breakdown fields due to their wide bandgap and the strain-induced piezoelectric charge leads to high carrier sheet densities at heterostructure interfaces [2]. The high electron mobility allows for high-frequency applications of these devices. More recently, HEMTs reached nanoscale gate lengths in order to dramatically increase cutoff and maximum oscillation frequency [3].

We investigate the quantum transport properties of high-frequency GaN high electron mobility transistors using a newly realized quantum transport model, that is part of the Vienna-Schrödinger-Poisson (VSP) quantum electronic simulation framework. Previous work [4] was based on 1D closed boundary Schrödinger-Poisson solvers and calculated the source-drain current a-posteriori [5]. In this work, we model a 2D/3D real-space Schrödinger system with open boundary conditions resulting in a consistent treatment of quantization and transport effects.

II. Quantum Transport Model

The quantum transport model is based on the quantum transmitting boundary method (QTBM) [6] and implemented in C++ within the VSP modeling framework [7]. Due to the generality of the code, the model is applicable to arbitrary device dimension, unstructured grids and arbitrary crystal

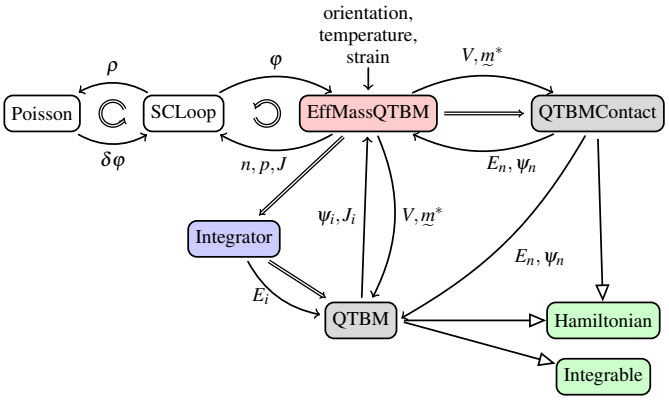

Figure 1. Schematic of the model setup. The self-consistent loop is managed by the *SCLoop* model which calls the *Poisson* model and the carrier model *EffMassQTBM* iteratively. *QTBMContact* determines the injecting contact modes; The *QTBM* model calculates the propagating waves, the carrier density, and the current density at a specific energy. Energy integration is managed by the *Integrator* class, which requires interface methods provided by *Integrable*. *QTBMContact* and *QTBM* inherit from the *Hamiltonian* class to consistently build the Hamiltonian matrix.

orientation rendering it useful for a wide range of applications. Using the QTBM formalism, we obtain the solution to

$$(\mathbf{H} - \mathscr{E}\mathbf{I} + \Sigma^{\mathrm{R}})\,|\Psi\rangle = |0\rangle\,. \tag{1}$$

To reduce computational effort, we do not solve the full system directly. At each energy, we first calculate the retarded Green's function of the unperturbed system

$$(\mathbf{H} - \mathscr{E}\mathbf{I})^{-1} := \mathbf{G}_{\mathbf{0}}^{\mathrm{R}}. \tag{2}$$

For that purpose, we start by LU factorizing the system

$$\mathbf{L}_{\mathbf{R}}\,\mathbf{U}_{\mathbf{R}} = \mathbf{H} - \mathscr{E}\mathbf{I}, \tag{3}$$

which needs to be done only once. We solve the system m times, once for each contact mode. The self-energy Σ^{R}, which is considered a low-rank update of the system, can be exactly accounted for by solving a condensed $m \times m$ system of equations. One obtains the wave functions ψ_i, the transmissions T_{ij} between mode i and j and the occupation, using a Fermi distribution for each contact. In a 2D device, the contribution of each mode i to the carrier density at a given energy $\mathscr{E}$ is written as

$$n_i(\mathbf{x}, \mathscr{E}) = \rho_{1\mathrm{D}}(\mathscr{E}, \mathscr{E}_i)\,|\psi_i(\mathbf{x})|^2 N_{\mathrm{C}} \mathrm{SF}(\mathscr{E}, \mathscr{E}_{\mathrm{F}}). \tag{4}$$

978-1-4799-5288-5/14/$31.00

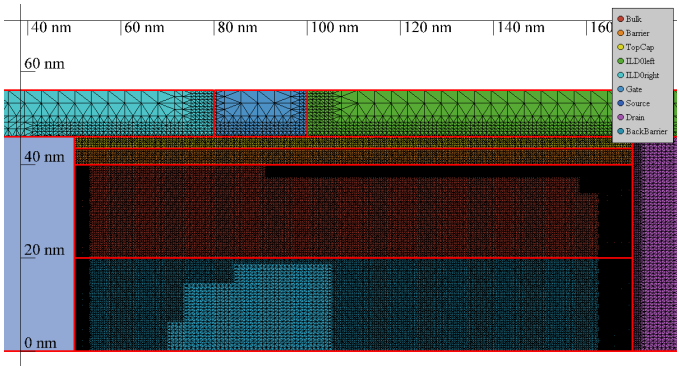

Figure 2. Structure of the GaN nanoscaled HEMT. The heterostructure consists of a top barrier with a 2.5 nm GaN capping layer on a 3.5 nm AlN barrier. The GaN channel is 20 nm thick and grown on an $Al_{0.08}Ga_{0.92}N$ back barrier to increase carrier confinement. The irregular mesh in the core device region is overlaid for illustration. To the left and right the extended, highly doped source and drain regions can be seen partially.

$\rho_{1D}(\mathscr{E},\mathscr{E}_i)$ is the energy-dependent 1D density of states of mode i, N_C is the effective density of states

$$N_C = \sqrt{\frac{m^*_{dos} k_B T}{2\pi\hbar^2}}, \tag{5}$$

and SF is the supply function for a 1D carrier gas defined as

$$\mathrm{SF}(\mathscr{E},\mathscr{E}_F) = F_{-1/2}(\mathscr{E},\mathscr{E}_F). \tag{6}$$

To calculate the total carrier density n and current density J, an energy integration is necessary. For that purpose, we developed an adaptive *Integrator* module based on our previous work [8], that automatically refines the energy grid, where needed. As quadrature rule we apply the Clenshaw-Curtis formula [9], which does not suffer from Runge's phenomenon.

The schematic structure of the model, the simulation flow, and the data interdependencies are depicted in Fig. 1. The self-consistent loop is managed by the *SCLoop* model which calls the *Poisson* model and the carrier model *EffMassQTBM* iteratively. The carrier model calls *QTBMContact* to determine the injecting contact modes. The propagating waves throughout the device, the carrier density, and the current density at a specific energy are determined by the *QTBM* model. The energy integration is managed by the *Integrator* class, which requires interface methods provided by *Integrable*. *QTBMContact* and *QTBM* inherit the description of the Schrödinger equation from the *Hamiltonian* class. This modular approach ensures flexibility and extensibility of the transport model. Due to the computational efficiency of VSP and the quantum transport model all the simulations can be run on standard workstations.

III. Simulation Setup

We created a GaN HEMT test device based on the generation IV design from reference [3]. Structure creation and meshing was done with the tool GTS Structure [10]. The device features an asymmetric gate structure with 20 nm gate length, a gate to source distance of 20 nm, and a gate to drain distance of 80 nm. The top barrier consists of a 2.5 nm GaN capping layer on a 3.5 nm AlN barrier. The GaN channel is 20 nm thick and an $Al_{0.08}Ga_{0.92}N$ back barrier is used to increase carrier confinement in the channel. The device region is unintentionally n-doped, whereas the source and drain regions are highly n^+-doped. The final structure with the mesh, as used for the VSP simulation, is shown in Fig. 2.

GaN and AlGaN are materials forming dipoles across the crystal which leads to interface charge at heterojunctions. The charge forms due to the spontaneous and piezoelectric contributions of the polarization divergence. We consider the interface charge in the *Poisson* model and compute the heterointerface charge according to the formulas in [11]. The polarization charge density at an $Al_xGa_{1-x}N$/GaN interface is given by

$$\sigma_{\mathrm{AlGaN/GaN}} = P_{\mathrm{GaN}} - P_{\mathrm{AlGaN}} \tag{7}$$

$$= \left(P^{\mathrm{sp}}_{\mathrm{GaN}} + P^{\mathrm{pz}}_{\mathrm{GaN}}\right) - \left(P^{\mathrm{sp}}_{\mathrm{AlGaN}} + P^{\mathrm{pz}}_{\mathrm{AlGaN}}\right), \tag{8}$$

where P^{sp} and P^{pz} are the spontaneous and the piezoelectric polarization, respectively. The spontaneous polarization of $Al_xGa_{1-x}N$ alloys can be described by [11]

$$P^{\mathrm{sp}}_{\mathrm{AlGaN}}(x) = -0.090x - 0.034(1-x) + 0.021x(1-x). \tag{9}$$

The Pt metal gate and the GaN top capping layer form a Schottky barrier of 1.15 eV height [12]. The highly n-doped drain and source regions were modeled as a classical 3D electron gas in thermal equilibrium. The core region of the device is described by the QTBM model and the carriers are injected at the contact/device interface segments.

The device is capped by a silicon nitride insulator layer. The conduction and valence band offsets with respect to gallium nitride have been set to $\mathscr{E}_{\mathrm{CBO}} = 2.5\,\mathrm{eV}$ and $\mathscr{E}_{\mathrm{VBO}} = 0.6\,\mathrm{eV}$ (type II) according to [13].

IV. Results and Discussion

We investigate two cases for the enhancement-mode HEMT: (i) the heterostructure is strained and the full piezoelectric polarization takes effect; (ii) the interfaces are fully relaxed and no piezoelectric charge is induced. First, we calculate the self-consistent electron conduction band edge with a bias of $V_G = 0\,\mathrm{V}$ and $V_{DS} = 1.0\,\mathrm{V}$ for both cases (see Fig. 3). The corresponding electron density for the Gen-IV HEMT at this bias is shown in Fig. 4. For this device configuration, a channel forms even with zero gate bias, which is confirmed by the simulation result. In the strained device, the channel is fully formed. For the fully relaxed case, a higher potential barrier forms below the gate, leading to a reduced number of electrons there. This is also reflected in the current density through the device as depicted in Fig. 5. Due to the strong confinement induced by the piezoelectric interface charge in the strained device, the current is concentrated in the channel region near the barrier. In the relaxed device, a partial loss of confinement can be seen in the current density.

The energy-resolved electron carrier density spectrum on a cut along the channel below the AlN barrier is shown in Fig. 6. The carriers residing at the source and drain regions as well as the extent of the channel can be clearly seen.

A cut through the device at the middle of the gate illustrates the influence of the interface charges on the conduction band edge (Fig. 7). The charges induce a strong field bending the band edge down below the barrier. The Pt Schottky barrier is recognizable as well. Figure 8 shows a comparison of the

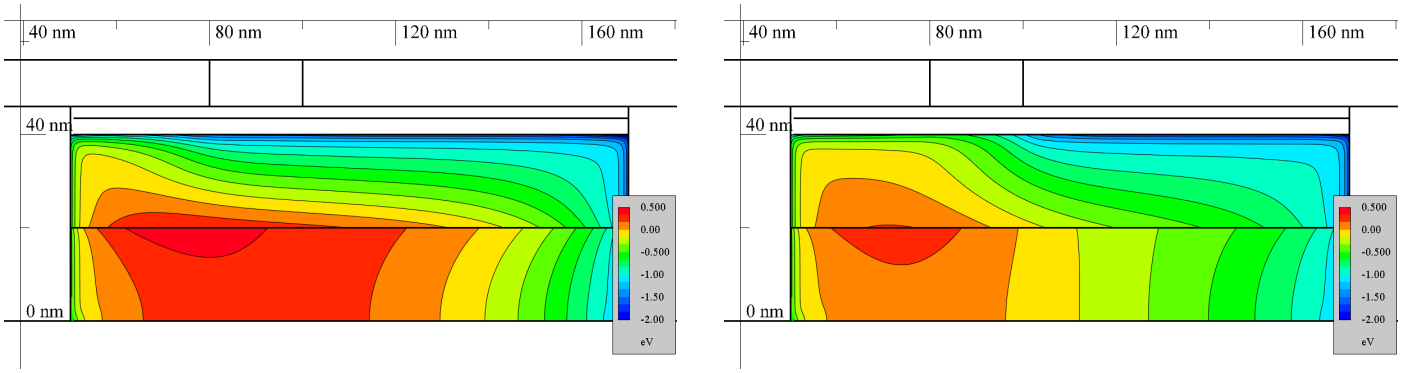

Figure 3. Self-consistent electron conduction band edge in the channel region calculated using the QTBM model at $V_G = 0\,V$ and $V_{DS} = 1\,V$; left: no strain relaxation is assumed and the full piezoelectric charge is taken into account; right: the heterostructure is fully relaxed and only spontaneous polarization is assumed.

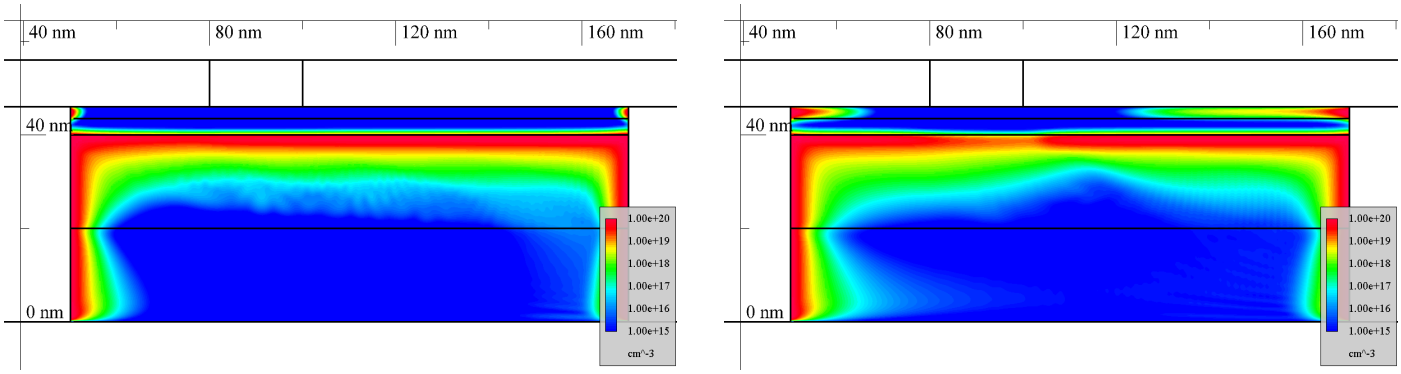

Figure 4. Self-consistent electron density in the channel region calculated using the QTBM model at $V_G = 0\,V$ and $V_{DS} = 1\,V$; left: no strain relaxation is assumed and the full piezoelectric charge is taken into account; right: the heterostructure is fully relaxed and only spontaneous polarization is assumed. Since this is an enhancement-mode device, the electrons form a channel directly below the AlN barrier region at this bias; Without relaxation the channel is fully formed, whereas for the relaxed device the influence of the gate potential can still be seen.

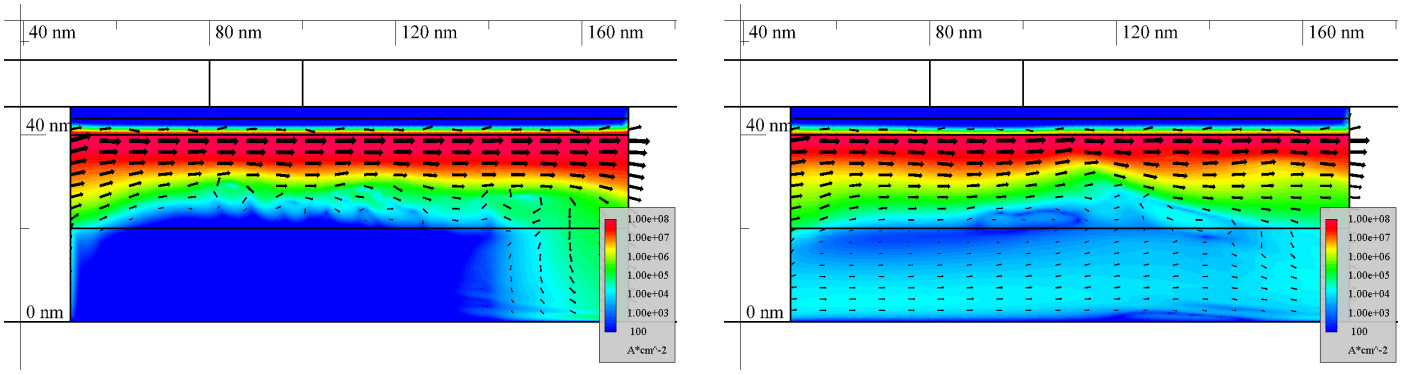

Figure 5. Self-consistent electron current density in the channel region calculated using the QTBM model at $V_G = 0\,V$ and $V_{DS} = 1\,V$; left: No strain relaxation is assumed and the full piezoelectric charge is taken into account; right: the heterostructure is fully relaxed and only spontaneous polarization is assumed. Due to a larger interface charge in the fully strained device, stronger confinement is achieved. In the relaxed device, part of the current is flowing through the back barrier region at a V_{DS} of 1 V already.

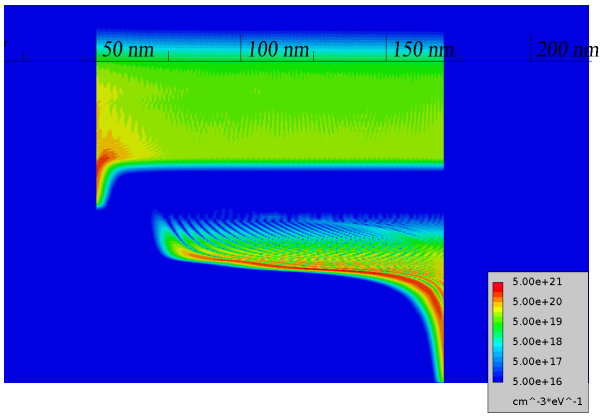

Figure 6. Energy-resolved electron carrier density spectrum at $V_G = 0\,V$ and $V_{DS} = 1.0\,V$ on a cut along the channel below the AlN barrier for an energy range from $-1.7\,eV$ to $0.4\,eV$.

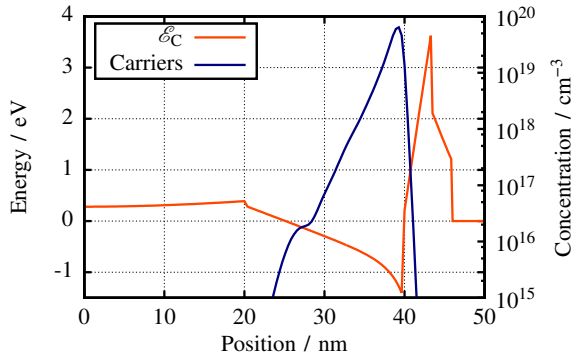

Figure 7. Self-consistently calculated conduction band edge and carrier concentration at $V_G = 0\,V$ and $V_{DS} = 1.0\,V$ on a cut centered at the gate.

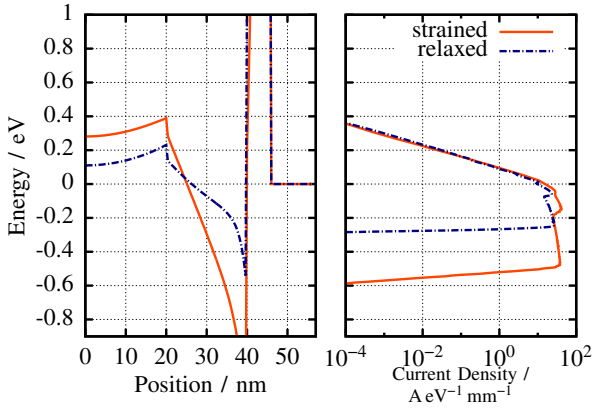

Figure 8. Left: conduction band edge on a cut centered at the gate; right: energy resolved source-drain current density. The HEMT was biased at $V_G = 0\,V$ and $V_{DS} = 1.0\,V$. The confinement is reduced in the relaxed device.

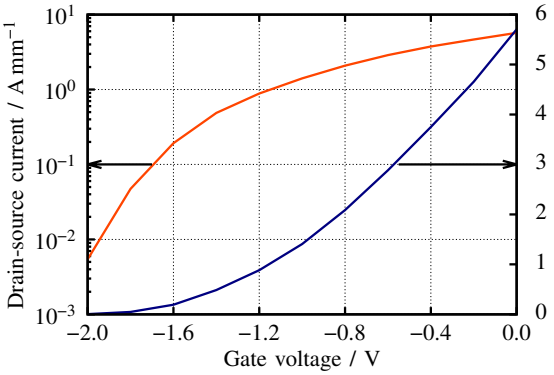

Figure 9. Current-voltage characteristics for the relaxed device at $V_{DS} = 1.0\,V$

energy resolved source-drain current density for the strained and relaxed device. As expected, the current is confined to the channel for the strained device. In the relaxed device, the well is smaller and there is considerable current flow above it. The transfer characteristics are depicted in Fig. 9.

V. Conclusion

We presented a quantum transport model for arbitrary device dimensions, unstructured grids, arbitrary materials and crystal orientation. We used the model to investigate a deeply scaled gallium nitride high electron mobility transistor and calculated self-consistent electronic band edges, carrier concentrations and ballistic currents. We have shown the influence of strain relaxation on the current density and carrier confinement.

Acknowledgment

This work has been supported by the Austrian Science Fund FFG project n° 838551 (NeGFQTS).

References

[1] U. K. Mishra *et al.*, "AlGaN/GaN HEMTs-an overview of device operation and applications," *Proceedings of the IEEE*, vol. 90, no. 6, pp. 1022–1031, 6 2002.

[2] S. Sheppard *et al.*, "High-power microwave GaN/AlGaN HEMTs on semi-insulating silicon carbide substrates," *IEEE Electron Device Letters*, vol. 20, no. 4, pp. 161–163, 4 1999.

[3] K. Shinohara *et al.*, "Scaling of GaN HEMTs and Schottky Diodes for Submillimeter-Wave MMIC Applications," *IEEE T. Electron. Dev.*, vol. 60, no. 10, pp. 2982–2996, Oct 2013.

[4] Y. Chang *et al.*, "Numerical simulation of current-voltage characteristics of AlGaN/GaN HEMTs at high temperatures," *Semicond. Sci. Technol.*, vol. 20, no. 2, p. 188, 2005.

[5] F. Sacconi *et al.*, "Spontaneous and piezoelectric polarization effects on the output characteristics of AlGaN/GaN heterojunction modulation doped FETs," *IEEE T. Electron. Dev.*, vol. 48, no. 3, pp. 450–457, Mar 2001.

[6] C. S. Lent and D. J. Kirkner, "The Quantum Transmitting Boundary Method," *J. Appl. Phys.*, vol. 67, no. 10, pp. 6353–6359, 5 1990.

[7] O. Baumgartner *et al.*, "VSP—a quantum-electronic simulation framework," *J. Comput. Electron.*, vol. 12, no. 4, pp. 701–721, 2013.

[8] ——, "Modeling of High-k-Metal-Gate-Stacks Using the Non-Equilibrium Green's Function Formalism," in *Proc. SISPAD*, 9 2008, pp. 353–356.

[9] C. W. Clenshaw and A. R. Curtis, "A Method for Numerical Integration on an Automatic Computer," *Num. Math.*, vol. 2, pp. 197–205, 1960.

[10] "GTS Framework," http://www.globaltcad.com/en/products/gts-framework.html.

[11] O. Ambacher *et al.*, "Electronics and sensors based on pyroelectric AlGaN/GaN heterostructures," *physica status solidi (c)*, vol. 0, no. 6, pp. 1878–1907, 2003.

[12] J. Schalwig *et al.*, "Hydrogen response mechanism of Pt-GaN Schottky diodes," *Applied Physics Letters*, vol. 80, no. 7, pp. 1222–1224, 2002.

[13] T. E. Cook *et al.*, "Band offset measurements of the Si3N4/GaN(0001) interface," *Journal of Applied Physics*, vol. 94, no. 6, pp. 3949–3954, 2003.